Astrophysical Constraints on the Symmetry Energy and the Neutron Skin of ^{208}Pb with Minimal Modeling Assumptions

Reed Essick,[1,2,*] Ingo Tews,[3,†] Philippe Landry,[4,‡] and Achim Schwenk[5,6,7,§]

[1]*Perimeter Institute for Theoretical Physics, 31 Caroline Street North, Waterloo, Ontario, Canada N2L 2Y5*
[2]*Kavli Institute for Cosmological Physics, The University of Chicago, Chicago, Illinois 60637, USA*
[3]*Theoretical Division, Los Alamos National Laboratory, Los Alamos, New Mexico 87545, USA*
[4]*Gravitational-Wave Physics & Astronomy Center, California State University, Fullerton, 800 N State College Blvd, Fullerton, California 92831, USA*
[5]*Technische Universität Darmstadt, Department of Physics, 64289 Darmstadt, Germany*
[6]*ExtreMe Matter Institute EMMI, GSI Helmholtzzentrum für Schwerionenforschung GmbH, 64291 Darmstadt, Germany*
[7]*Max-Planck-Institut für Kernphysik, Saupfercheckweg 1, 69117 Heidelberg, Germany*

(Received 21 February 2021; revised 3 September 2021; accepted 14 September 2021; published 2 November 2021)

The symmetry energy and its density dependence are crucial inputs for many nuclear physics and astrophysics applications, as they determine properties ranging from the neutron-skin thickness of nuclei to the crust thickness and the radius of neutron stars. Recently, PREX-II reported a value of 0.283 ± 0.071 fm for the neutron-skin thickness of ^{208}Pb, implying a slope parameter $L = 106 \pm 37$ MeV, larger than most ranges obtained from microscopic calculations and other nuclear experiments. We use a nonparametric equation of state representation based on Gaussian processes to constrain the symmetry energy S_0, L, and $R_{\rm skin}^{^{208}\rm Pb}$ directly from observations of neutron stars with minimal modeling assumptions. The resulting astrophysical constraints from heavy pulsar masses, LIGO/Virgo, and NICER clearly favor smaller values of the neutron skin and L, as well as negative symmetry incompressibilities. Combining astrophysical data with PREX-II and chiral effective field theory constraints yields $S_0 = 33.0^{+2.0}_{-1.8}$ MeV, $L = 53^{+14}_{-15}$ MeV, and $R_{\rm skin}^{^{208}\rm Pb} = 0.17^{+0.04}_{-0.04}$ fm.

DOI: 10.1103/PhysRevLett.127.192701

Introduction.—The symmetry energy $S(n)$ is a central quantity in nuclear physics and astrophysics. It characterizes the change in the nuclear-matter energy as the ratio of protons to neutrons is varied and thus impacts, e.g., the neutron-skin thickness of nuclei [1–3], their dipole polarizability [4,5], and the radius of neutron stars (NSs) [6,7]. This information is encoded in the nuclear equation of state (EOS), described by the nucleonic energy per particle, $E_{\rm nuc}/A$, a function of total baryon density n and proton fraction $x = n_p/n$ for proton density n_p. The energy per particle is connected to the bulk properties of atomic nuclei for proton fractions close to $x = 1/2$, i.e., symmetric nuclear matter (SNM) with $E_{\rm SNM}/A = (E_{\rm nuc}/A)|_{x=1/2}$. As the neutron-proton asymmetry increases (or the proton fraction x decreases) the energy per particle increases, reaching a maximum for $x = 0$, i.e., pure neutron matter (PNM) with $E_{\rm PNM}/A = (E_{\rm nuc}/A)|_{x=0}$. PNM is closely related to NS matter. The symmetry energy characterizes the difference between these two systems:

$$S(n) = \frac{E_{\rm PNM}}{A}(n) - \frac{E_{\rm SNM}}{A}(n). \qquad (1)$$

Crucial information is encoded in the density dependence of $S(n)$, which is captured by the slope parameter L and the curvature $K_{\rm sym}$ defined at nuclear saturation density, $n_0 \approx 0.16\ {\rm fm}^{-3}$,

$$L = 3n\frac{\partial S(n)}{\partial n}\bigg|_{n_0}, \qquad K_{\rm sym}(n) = 9n^2\frac{\partial^2 S(n)}{\partial n^2}\bigg|_{n_0}. \qquad (2)$$

As $d(E_{\rm SNM}/A)/dn = 0$ at n_0, L describes the pressure of PNM around n_0. $S_0 = S(n_0)$ and L are of great interest to nuclear physics [5,8,9] and astrophysics [10–12]. Experimental [4,5,13,14] and theoretical [15–18] determinations consistently place S_0 in the range of 30–35 MeV and L in the range of 30–70 MeV. Recently, however, the PREX-II experiment reported a new result for the neutron-skin thickness of ^{208}Pb [19], $R_{\rm skin}^{^{208}\rm Pb}$, a quantity strongly correlated with L (see, e.g., Refs. [1–3]). The measurement of $R_{\rm skin}^{^{208}\rm Pb} = 0.283 \pm 0.071$ fm (mean $\pm$ standard deviation), including PREX-I and PREX-II data, led Ref. [20] to conclude that $L = 106 \pm 37$ MeV. This value is larger than previous determinations, and thus presents a challenge to our understanding of nuclear matter, should a high L value be confirmed precisely.

In this Letter, we address this question by constraining S_0, its density dependence L, and $R_{\rm skin}^{^{208}\rm Pb}$ directly from astrophysical observations. We adopt a nonparametric representation for the EOS [21,22] to minimize the model dependence of the analysis, in contrast to other astrophysical inferences, e.g., Refs. [23–26]. Nonparametric inference allows us to explore a multitude of EOSs that are informed *only* by a NS crust model at densities $n < 0.3n_0$, where the EOS uncertainty is small, combined with the requirements of causality and thermodynamic stability at higher densities. Following Ref. [27], the possible EOSs are weighed based on their compatibility with gravitational-wave (GW) and electromagnetic observations of NSs (massive pulsars and x-ray timing with NICER). By calculating S_0, L, $K_{\rm sym}$, and $R_{\rm skin}^{^{208}\rm Pb}$ for each of these EOSs, we obtain astrophysically informed posterior distributions for these key nuclear properties. Furthermore, we study how L and $R_{\rm skin}^{^{208}\rm Pb}$ change as constraints from nuclear theory are included up to progressively higher densities.

Nonparametric inference for the EOS.—We connect NS observables to S_0, L, and $K_{\rm sym}$ using a nonparametric representation of the EOS based on Gaussian processes (GPs) [21,22]. The GPs model the uncertainty in the correlations between the sound speed in β equilibrium at different pressures, but do not specify the exact functional form of the EOS, unlike other parametrizations [28–36]. The nonparametric EOSs consequently exhibit a wider range of behavior than parametric EOSs, mitigating the impact of modeling assumptions. The nonparametric EOS inference proceeds through Monte Carlo sampling from a prior constructed as a mixture of GPs to obtain a large set of EOS realizations. Each EOS is then compared to astrophysical observations via optimized kernel density estimates (KDEs) of the likelihoods, resulting in a discrete representation of the posterior EOS process as a list of weighted samples (see Refs. [22,27] for more details). The posterior probability of a given EOS realization, which we label by its energy density ε_β, is calculated as

$$P(\varepsilon_\beta|\{d\}) \propto P(\varepsilon_\beta)\prod_i P(d_i|\varepsilon_\beta), \qquad (3)$$

where $\{d\} = \{d_1, d_2, \ldots\}$ is the set of observations, $P(d_i|\varepsilon_\beta)$ are the corresponding likelihood models, and $P(\varepsilon_\beta)$ is the EOS realization's prior probability. The specific likelihoods used in this work are as follows: (a) Pulsar timing measurements of masses for the two heaviest known NSs (PSR J0740 + 6620 [37,38], PSR J0348 + 0432 [39]) modeled as Gaussian distributions with means and standard deviations $2.08 \pm 0.07\ M_\odot$ and $2.01 \pm 0.04\ M_\odot$, respectively; (b) GW measurements of masses and tidal deformabilities in the binary NS merger GW170817 [40] from Advanced LIGO [41] and Virgo [42]; and (c) x-ray pulse-profile measurements of PSR J0030 + 0451's mass and radius assuming a three-hotspot configuration [43] (see also Ref. [44], which yields comparable results [27]).

Our basic nonparametric prior can also be conditioned self-consistently on theoretical calculations of the EOS at nuclear densities, while retaining complete model freedom at higher densities [45]. Here we marginalize over the uncertainty bands from four different chiral effective field theory (χEFT) calculations: quantum Monte Carlo calculations using local χEFT interactions up to next-to-next-to-leading order (N^{2}LO) [46], many-body perturbation theory (MBPT) calculations using nonlocal χEFT interactions up to next-to-next-to-next-to-leading order (N^{3}LO) of Refs. [16,47], and MBPT calculations with two-nucleon interactions at N^{3}LO and three-nucleon interactions at N^{2}LO (based on a broader range of three-nucleon couplings) [31,48]. The resulting marginalized χEFT band overlaps with results for other realistic Hamiltonians, particularly for Argonne- and Urbana-type interactions [49]. This allows us to account for different nuclear interactions and many-body approaches, increasing the robustness of our results.

To translate the EOS posterior process into distributions for the nuclear physics properties, we establish a probabilistic map from ε_β to $E_{\rm PNM}/A$, S_0, L, and $K_{\rm sym}$ (described below). Marginalization over the EOS then yields a posterior

$$P(E_{\rm PNM}/A, S_0, L, K_{\rm sym}|\{d\}) = \int \mathcal{D}\varepsilon_\beta P(\varepsilon_\beta|\{d\}) P(E_{\rm PNM}/A, S_0, L, K_{\rm sym}|\varepsilon_\beta), \qquad (4)$$

informed by the astrophysical observations. Constraints on $R_{\rm skin}^{^{208}\rm Pb}$ are obtained from empirical correlations with L [50], calculated from a broad range of nonrelativistic Skyrme and relativistic mean-field density functionals; see also Refs. [1,3]. To account for the theoretical uncertainty in the fit of Ref. [2] and mitigate its model dependence (cf. Refs. [13,50,51]), we adopt a probabilistic mapping: $P(R_{\rm skin}^{^{208}\rm Pb}|L) = \mathcal{N}(\mu_R, \sigma_R)$ with $\mu_R(L)[{\rm fm}] = 0.072 + 0.00194 \times (L[{\rm MeV}])$ and $\sigma_R = 0.0143$ fm.

Reconstructing the symmetry energy.—Because our nonparametric EOS realizations are not formulated in terms of S_0, L, or $K_{\rm sym}$, we discuss how to extract the nuclear parameters near n_0 directly from the EOS; see the Supplemental Material [52] for more details. The nonparametric inference provides the individual EOSs in terms of the baryon density n as well as the pressure p_β and energy density ε_β in β equilibrium. Each realization is matched to the BPS crust [53] around $0.3n_0$. The choice of a single crust at low densities does not affect our conclusions; see Sec. V of Ref. [54]. The EOS quantities are related to $E_{\rm nuc}/A$ through $\varepsilon = n(E_{\rm nuc}/A + m_N)$ with the average nucleon mass m_N. To reconstruct $E_{\rm nuc}/A$, we correct ε_β by the electron contribution ε_e,

$$\frac{E_{\rm nuc}}{A}(n, x) = \frac{\varepsilon_\beta(n) - \varepsilon_e(n, x)}{n} - m_N. \qquad (5)$$

The proton fraction $x(n)$ is unknown and needs to be determined self-consistently for each EOS by enforcing

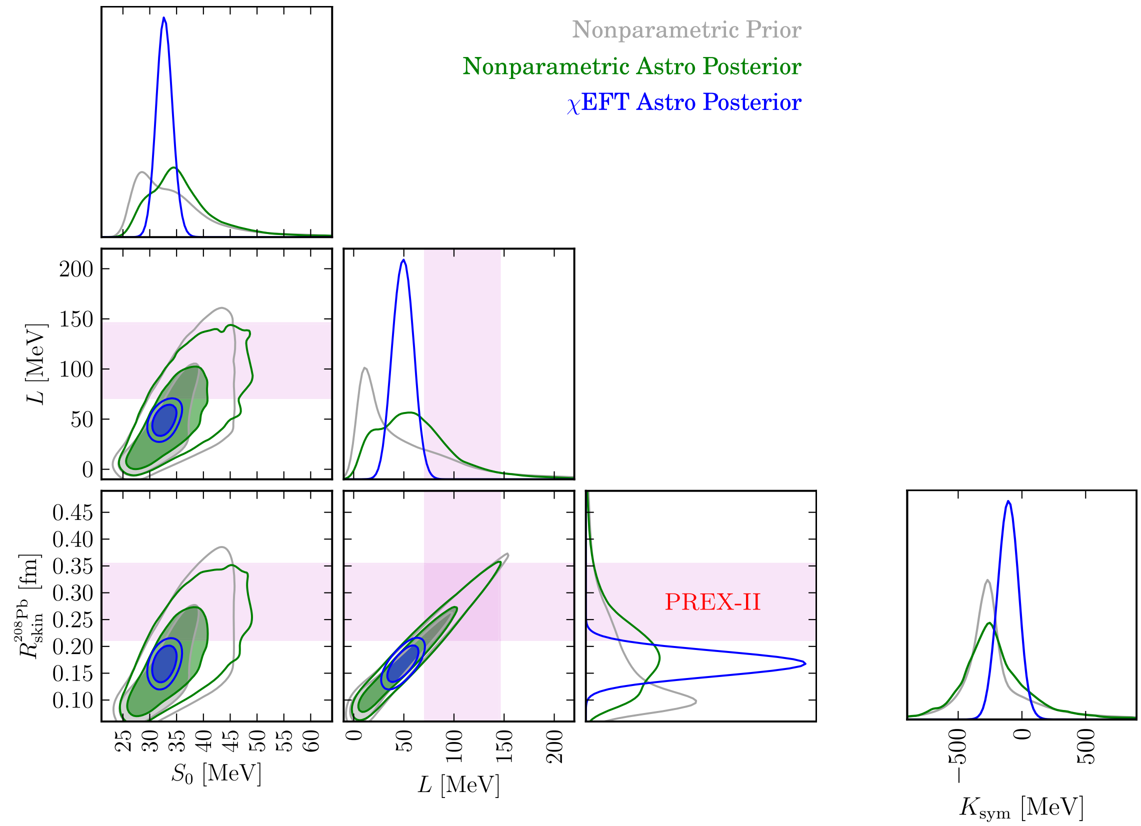

FIG. 1. Correlations between the symmetry energy S_0, the slope parameter L, and the neutron-skin thickness of ^{208}Pb $R_{\rm skin}^{208\rm Pb}$. We show the nonparametric prior (gray), the nonparametric posterior conditioned on astrophysical observations (green), and the nonparametric posterior conditioned on an average over four χEFT calculations (up to $\approx n_0$) and astrophysical observations (blue). Joint distributions show the 68% (shaded) and 90% (solid lines) credible regions. Shaded bands (pink) show the approximate 68% credible region for parameters constrained by PREX-II: $R_{\rm skin}^{208\rm Pb}$ [19] and the resulting constraints on L using the correlation from Ref. [50]. Note how the inclusion of the astrophysical observations shifts the peak in the marginal distributions for S_0, L, and $R_{\rm skin}^{208\rm Pb}$, a trend that is reinforced by the addition of χEFT information. We also show the one-dimensional marginal distributions for the symmetry incompressibility $K_{\rm sym}$ in a separate panel.

β equilibrium, $\mu_n(n,x) = \mu_p(n,x) + \mu_e(n,x)$, where $\mu_i(n,x)$ is the chemical potential for particle species i. This leads to the condition for β equilibrium (see Ref. [31] and the Supplemental Material [52] for details),

$$0 = m_n - m_p - \frac{\partial(E_{\rm nuc}/A)}{\partial x} - \mu_e(n,x). \qquad (6)$$

To extract the symmetry energy from each EOS realization, we need to know the dependence of $E_{\rm nuc}/A$ with proton fraction. Here, we approximate the x dependence using the standard quadratic expansion,

$$\frac{E_{\rm nuc}}{A}(n,x) = \frac{E_{\rm SNM}}{A}(n) + S(n)(1-2x)^2. \qquad (7)$$

Nonquadratic terms are small at n_0 and can be neglected given current EOS uncertainties [55,56]. Because we only work around n_0, we can characterize the SNM energy using the standard expansion,

$$\frac{E_{\rm SNM}}{A}(n) = E_0 + \frac{1}{2}K_0\left(\frac{n-n_0}{3n_0}\right)^2 + \cdots, \qquad (8)$$

where uncertainty in the saturation energy E_0, n_0, and the incompressibility K_0 is based on the empirical ranges from Ref. [9]. Combining Eqs. (1) and Eqs. (5)–(8), we find that β equilibrium must satisfy

$$\frac{1-2x_\beta}{4}[m_p - m_n + \mu_e(n,x_\beta)] = \frac{\varepsilon_\beta(n) - \varepsilon_e(n,x_\beta)}{n} - m_{\rm N} - \frac{E_{\rm SNM}}{A}(n). \qquad (9)$$

We use the relations for a relativistic Fermi gas for the electron energy density and chemical potential [57].

To summarize, given a nonparametric EOS realization and a sample from the empirical distribution for each of the parameters E_0, K_0, and n_0, we reconstruct the proton fraction in β equilibrium x_β self-consistently at each density around nuclear saturation. We then calculate $E_{\rm PNM}/A$, S_0,

TABLE I. Medians and 90% highest-probability-density credible regions for the studied nuclear properties. We compute $R_{\rm skin}^{^{208}{\rm Pb}}$ from L using the linear fit reported in Ref. [50], approximating the uncertainty in the fit as described in the text.

	$E_{\rm PNM}/A$ [MeV]	S_0 [MeV]	L [MeV]	$K_{\rm sym}$ [MeV]	$R_{\rm skin}^{^{208}{\rm Pb}}$ [fm]
Nonparametric prior	$17.5^{+14.6}_{-7.7}$	$33.3^{+14.7}_{-8.2}$	38^{+109}_{-41}	-255^{+853}_{-566}	$0.14^{+0.19}_{-0.09}$
Nonparametric Astro posterior	$19.3^{+11.7}_{-8.5}$	$35.1^{+11.6}_{-8.9}$	58^{+61}_{-56}	-240^{+559}_{-503}	$0.19^{+0.12}_{-0.11}$
Nonparametric Astro + PREX-II posterior	$21.5^{+10.8}_{-8.3}$	$37.3^{+11.8}_{-7.5}$	80^{+51}_{-46}	-223^{+608}_{-565}	$0.23^{+0.10}_{-0.10}$
χEFT Astro posterior	$16.9^{+1.5}_{-1.4}$	$32.7^{+1.9}_{-1.8}$	49^{+14}_{-15}	-107^{+124}_{-128}	$0.17^{+0.04}_{-0.04}$
χEFT Astro + PREX-II posterior	$17.1^{+1.5}_{-1.5}$	$33.0^{+2.0}_{-1.8}$	53^{+14}_{-15}	-91^{+118}_{-130}	$0.17^{+0.04}_{-0.04}$

L, and $K_{\rm sym}$ as a function of n and report their values at the reference density $n_0^{(\rm ref)} = 0.16\ {\rm fm}^{-3}$. The neutron-skin thickness is estimated via the empirical fit between $R_{\rm skin}^{^{208}{\rm Pb}}$ and L, as discussed above.

Results and discussion.—The constraints on S_0, L, $K_{\rm sym}$, and $R_{\rm skin}^{^{208}{\rm Pb}}$ are shown in Fig. 1. We plot the nonparametric prior, the posterior constrained by astrophysical data, and the posterior additionally constrained by the χEFT calculations up to $n \approx n_0$. As our GPs are conditioned on χEFT up to a maximum pressure ($p_{\rm max}$), we report the median density at that pressure (the exact density at $p_{\rm max}$ varies due to uncertainty in the EOS from χEFT). Prior and posterior credible regions are provided in Table I. We find that the PREX-II result for $R_{\rm skin}^{^{208}{\rm Pb}}$ and the extracted range for L of Ref. [20], 73–147 MeV at 1σ, are in mild tension with the GP conditioned on χEFT calculations up to n_0, while the GP conditioned only on astrophysical observations is consistent with both results and cannot resolve any tension due to its large uncertainties. However, the Astro-only and χEFT posteriors peak at similar values for L (55–65 MeV), below the PREX-II result. The astrophysical data do not strongly constrain $K_{\rm sym}$, but suggest it is negative.

In Fig. 2, we show the evolution of our constraints on L and $R_{\rm skin}^{^{208}{\rm Pb}}$ as a function of the maximum density up to which we condition on χEFT, from no conditioning on χEFT to conditioning on χEFT up to n_0. The more we trust χEFT constraints, the larger the tension with PREX-II results becomes. We estimate a 12.3% probability (p value) that the true $R_{\rm skin}^{^{208}{\rm Pb}}$ differs from the PREX-II mean by at least as much as the Astro + χEFT posterior suggests, given the uncertainty in PREX-II's measurement. However, if a hypothetical experiment confirmed the PREX-II mean with half the uncertainty, this p value would be reduced to 0.6%. We also show the estimate for $R_{\rm skin}^{^{208}{\rm Pb}}$ obtained from an analysis of dipole polarizability data ($\alpha_D^{^{208}{\rm Pb}}$, [13]), which finds $R_{\rm skin}^{^{208}{\rm Pb}} = 0.13$–$0.19$ fm. The latter agrees very well with both the χEFT results and the nonparametric GP. See Ref. [54] for more comparisons, including joint constraints with both $R_{\rm skin}^{^{208}{\rm Pb}}$ and $\alpha_D^{^{208}{\rm Pb}}$.

In Fig. 3, we present the modeled correlation between L and $R_{\rm skin}^{^{208}{\rm Pb}}$ as well as the radius of a 1.4 $M_\odot$ NS, $R_{1.4}$. Besides those shared with Fig. 1, we show posteriors that are also conditioned on the PREX-II result. Even though the results for L and $R_{\rm skin}^{^{208}{\rm Pb}}$ are very different for the various constraints, $R_{1.4}$ does not significantly change. Indeed, the mapping from L to $R_{1.4}$ is broader than often assumed [6], and we find that $R_{1.4}$ is nearly independent of our range for L. Hence, the findings of Ref. [20], indicating that PREX-II requires large radii, include some model dependence.

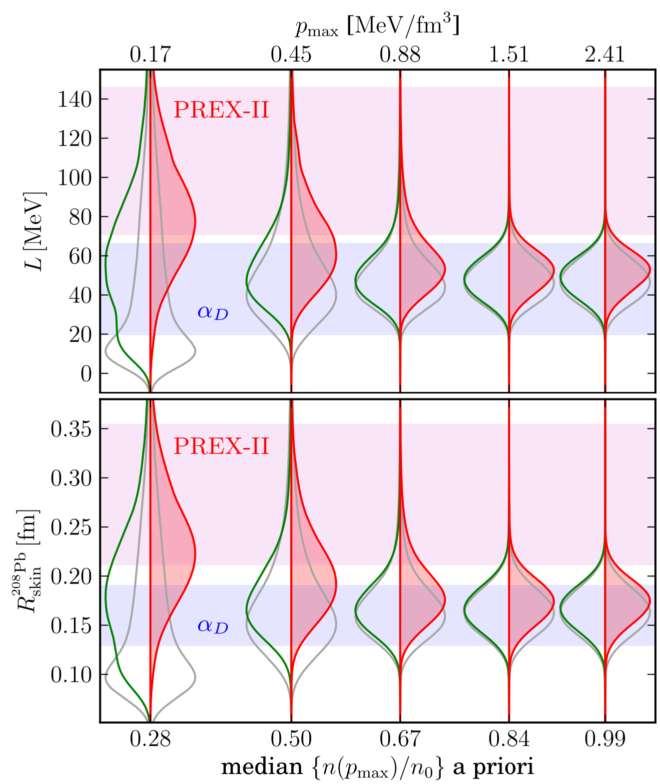

FIG. 2. Prior (gray, unshaded), Astro posterior (green, left-unshaded), and Astro + PREX-II posterior (red, right-shaded) distributions for L (top) and $R_{\rm skin}^{^{208}{\rm Pb}}$ (bottom) as a function of the maximum pressure (top axis) or density (bottom axis) up to which we trust theoretical nuclear-physics predictions from χEFT (see text for details). Shaded bands show the approximate 68% credible region from PREX-II [19] (pink) and from Ref. [13] based on the electric dipole polarizability α_D (light blue).

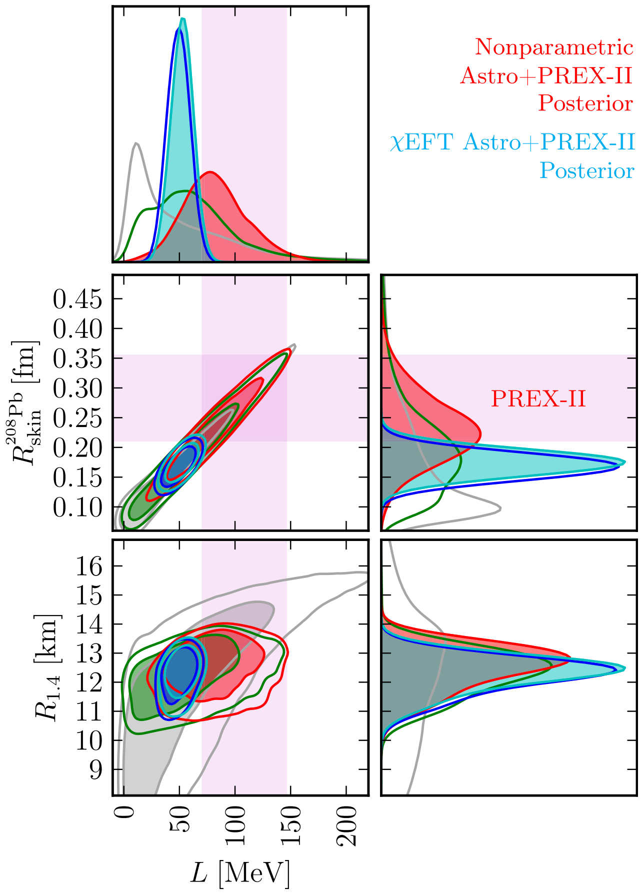

FIG. 3. Correlations between $R_{\rm skin}^{208\rm Pb}$, L, and the radius of a 1.4 $M_\odot$ NS, $R_{1.4}$. In addition to the priors and posteriors shown in Fig. 1, we show the nonparametric (red) and χEFT (trusted up to n_0; light blue) posteriors conditioned on both astrophysical observations and PREX-II. Astro + PREX-II posteriors are shaded in the one-dimensional distributions to distinguish them from the Astro-only posteriors. Joint distributions show the 68% (shaded) and 90% (solid lines) credible regions. Shaded bands (pink) show the approximate 68% credible region from PREX-II.

Given the mild tension between the PREX-II value of $R_{\rm skin}^{208\rm Pb}$ and that inferred from the astrophysical inference with χEFT information, we investigate what kind of EOS behavior is required to satisfy both the PREX-II and astrophysical constraints. In Fig. 4 we show the speed of sound c_s as a function of density for the nonparametric GP conditioned only on astrophysical data for all values of L, for 30 MeV $< L \leq 70$ MeV, and for $L > 100$ MeV. We find that the speed of sound generally increases with density. However, if we assume $L > 100$ MeV, we find a local maximum in the median $c_s(n)$ just below n_0, although the uncertainties in c_s are large. The reason for this feature is that EOSs that are stiff at low densities (large L) need to soften beyond n_0 to remain consistent with astrophysical data from GW observations, in particular GW170817. Should the PREX-II constraints be confirmed

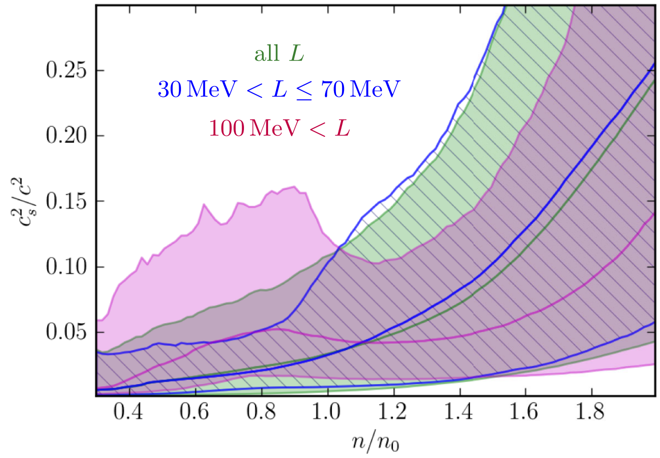

FIG. 4. Median and 90% one-dimensional symmetric posterior credible regions for c_s^2 at each density n with astrophysical observations for all L (shaded green), 30 MeV $< L \leq 70$ MeV (unshaded blue hatches), and 100 MeV $< L$ (shaded purple).

with smaller uncertainty in the future, this might favor the existence of a phase transition between $1-2n_0$.

In summary, we have used nonparametric GP EOS inference to constrain the symmetry energy, its density dependence, and $R_{\rm skin}^{208\rm Pb}$ directly from astrophysical data, leading to $S_0 = 35.1^{+11.6}_{-8.9}$ MeV, $L = 58^{+61}_{-56}$ MeV, and $R_{\rm skin}^{208\rm Pb} = 0.19^{+0.12}_{-0.11}$ fm. Folding in χEFT constraints reduces these ranges to $S_0 = 32.7^{+1.9}_{-1.8}$ MeV, $L = 49^{+14}_{-15}$ MeV, and $R_{\rm skin}^{208\rm Pb} = 0.17^{+0.04}_{-0.04}$ fm. While these results prefer values below the recent PREX-II values [19,20], in good agreement with other nuclear physics information, the PREX-II uncertainties are still broad and any tension is mild. Our nonparametric analysis suggests that a $R_{\rm skin}^{208\rm Pb}$ uncertainty of ± 0.04 fm could challenge astrophysical and χEFT constraints. Note that the formation of light clusters at the surface of heavy nuclei could affect the extracted L value [58]. Finally, our results demonstrate that the correlation between $R_{1.4}$ and L (or $R_{\rm skin}^{208\rm Pb}$) is looser than analyses based on a specific class of EOS models would suggest. Extrapolating neutron-skin thickness measurements to NS scales thus requires a careful treatment of systematic EOS model uncertainties. In particular, the PREX-II result does not require large NS radii. However, if the high L values of PREX-II persist, this may suggest a peak in the sound speed around saturation density.

R. E. was supported by the Perimeter Institute for Theoretical Physics and the Kavli Institute for Cosmological Physics. R. E. thanks the Canadian Institute for Advanced Research (CIFAR) for support. Research at Perimeter Institute is supported in part by the Government of Canada through the Department of Innovation, Science and Economic Development Canada and by the Province of Ontario through the Ministry of Colleges and Universities.

The Kavli Institute for Cosmological Physics at the University of Chicago is supported by an endowment from the Kavli Foundation and its founder Fred Kavli. The work of I. T. was supported by the U.S. Department of Energy, Office of Science, Office of Nuclear Physics, under Contract No. DE-AC52-06NA25396, by the Laboratory Directed Research and Development program of Los Alamos National Laboratory under Projects No. 20190617PRD1 and No. 20190021DR, and by the U.S. Department of Energy, Office of Science, Office of Advanced Scientific Computing Research, Scientific Discovery through Advanced Computing (SciDAC) NUCLEI program. P. L. is supported by National Science Foundation Grant No. PHY-1836734 and by a gift from the Dan Black Family Foundation to the Gravitational-Wave Physics & Astronomy Center. The work of A. S. was supported in part by the Deutsche Forschungsgemeinschaft (DFG, German Research Foundation) - Project-ID 279384907 - SFB 1245. This work benefitted from discussions within IReNA, which is supported in part by the National Science Foundation under Grant No. OISE-1927130. The authors also gratefully acknowledge the computational resources provided by the LIGO Laboratory and supported by NSF Grants No. PHY-0757058 and No. PHY-0823459. Computational resources have also been provided by the Los Alamos National Laboratory Institutional Computing Program, which is supported by the U.S. Department of Energy National Nuclear Security Administration under Contract No. 89233218CNA000001, and by the National Energy Research Scientific Computing Center (NERSC), which is supported by the U.S. Department of Energy, Office of Science, under Contract No. DE-AC02-05CH11231.

[*]reed.essick@gmail.com
[†]itews@lanl.gov
[‡]plandry@fullerton.edu
[§]schwenk@physik.tu-darmstadt.de

[1] S. Typel and B. A. Brown, Phys. Rev. C **64**, 027302 (2001).
[2] X. Viñas, M. Centelles, X. Roca-Maza, and M. Warda, Eur. Phys. J. A **50**, 27 (2014).
[3] P. G. Reinhard and W. Nazarewicz, Phys. Rev. C **93**, 051303 (R) (2016).
[4] A. Tamii, I. Poltoratska, P. von Neumann-Cosel, Y. Fujita, T. Adachi, C. A. Bertulani, J. Carter, M. Dozono, H. Fujita, K. Fujita *et al.*, Phys. Rev. Lett. **107**, 062502 (2011).
[5] J. M. Lattimer and Y. Lim, Astrophys. J. **771**, 51 (2013).
[6] J. M. Lattimer and M. Prakash, Astrophys. J. **550**, 426 (2001).
[7] A. W. Steiner and S. Gandolfi, Phys. Rev. Lett. **108**, 081102 (2012).
[8] M. B. Tsang, J. R. Stone, F. Camera, P. Danielewicz, S. Gandolfi, K. Hebeler, C. J. Horowitz, J. Lee, W. G. Lynch, Z. Kohley *et al.*, Phys. Rev. C **86**, 015803 (2012).
[9] S. Huth, C. Wellenhofer, and A. Schwenk, Phys. Rev. C **103**, 025803 (2021).
[10] K. Oyamatsu and K. Iida, Phys. Rev. C **75**, 015801 (2007).
[11] T. Fischer, M. Hempel, I. Sagert, Y. Suwa, and J. Schaffner-Bielich, Eur. Phys. J. A **50**, 46 (2014).
[12] D. Neill, W. G. Newton, and D. Tsang, Mon. Not. R. Astron. Soc. **504**, 1129 (2021).
[13] X. Roca-Maza, X. Viñas, M. Centelles, B. K. Agrawal, G. Colò, N. Paar, J. Piekarewicz, and D. Vretenar, Phys. Rev. C **92**, 064304 (2015).
[14] P. Russotto, S. Gannon, S. Kupny, P. Lasko, L. Acosta, M. Adamczyk, A. Al-Ajlan, M. Al-Garawi, S. Al-Homaidhi, F. Amorini *et al.*, Phys. Rev. C **94**, 034608 (2016).
[15] K. Hebeler, J. M. Lattimer, C. J. Pethick, and A. Schwenk, Phys. Rev. Lett. **105**, 161102 (2010).
[16] I. Tews, T. Krüger, K. Hebeler, and A. Schwenk, Phys. Rev. Lett. **110**, 032504 (2013).
[17] D. Lonardoni, I. Tews, S. Gandolfi, and J. Carlson, Phys. Rev. Research **2**, 022033(R) (2020).
[18] C. Drischler, R. J. Furnstahl, J. A. Melendez, and D. R. Phillips, Phys. Rev. Lett. **125**, 202702 (2020).
[19] D. Adhikari, H. Albataineh, D. Androic, K. Aniol, D. S. Armstrong, T. Averett, C. Ayerbe Gayoso, S. Barcus, V. Bellini, R. S. Beminiwattha *et al.* (PREX Collaboration), Phys. Rev. Lett. **126**, 172502 (2021).
[20] B. T. Reed, F. J. Fattoyev, C. J. Horowitz, and J. Piekarewicz, Phys. Rev. Lett. **126**, 172503 (2021).
[21] P. Landry and R. Essick, Phys. Rev. D **99**, 084049 (2019).
[22] R. Essick, P. Landry, and D. E. Holz, Phys. Rev. D **101**, 063007 (2020).
[23] N. Alam, B. K. Agrawal, M. Fortin, H. Pais, C. Providência, A. R. Raduta, and A. Sulaksono, Phys. Rev. C **94**, 052801 (R) (2016).
[24] Z. Carson, A. W. Steiner, and K. Yagi, Phys. Rev. D **99**, 043010 (2019).
[25] B. Biswas, P. Char, R. Nandi, and S. Bose, Phys. Rev. D **103**, 103015 (2021).
[26] T.-G. Yue, L.-W. Chen, Z. Zhang, and Y. Zhou, arXiv: 2102.05267.
[27] P. Landry, R. Essick, and K. Chatziioannou, Phys. Rev. D **101**, 123007 (2020).
[28] J. S. Read, B. D. Lackey, B. J. Owen, and J. L. Friedman, Phys. Rev. D **79**, 124032 (2009).
[29] L. Lindblom, Phys. Rev. D **82**, 103011 (2010).
[30] L. Lindblom and N. M. Indik, Phys. Rev. D **86**, 084003 (2012).
[31] K. Hebeler, J. Lattimer, C. Pethick, and A. Schwenk, Astrophys. J. **773**, 11 (2013).
[32] M. G. Alford, S. Han, and M. Prakash, Phys. Rev. D **88**, 083013 (2013).
[33] C. A. Raithel, F. Ozel, and D. Psaltis, Astrophys. J. **831**, 44 (2016).
[34] I. Tews, J. Carlson, S. Gandolfi, and S. Reddy, Astrophys. J. **860**, 149 (2018).
[35] I. Tews, J. Margueron, and S. Reddy, Phys. Rev. C **98**, 045804 (2018).
[36] S. Greif, G. Raaijmakers, K. Hebeler, A. Schwenk, and A. Watts, Mon. Not. R. Astron. Soc. **485**, 5363 (2019).
[37] H. T. Cromartie, E. Fonseca, S. M. Ransom, P. B. Demorest, Z. Arzoumanian, H. Blumer, P. R. Brook, M. E. DeCesar, T. Dolch, J. A. Ellis *et al.*, Nat. Astron. **4**, 72 (2020).
[38] E. Fonseca, H. T. Cromartie, T. T. Pennucci, P. S. Ray, A. Y. Kirichenko, S. M. Ransom, P. B. Demorest, I. H. Stairs,

Z. Arzoumanian, L. Guillemot *et al.*, Astrophys. J. Lett. **915**, L12 (2021).

[39] J. Antoniadis, P. C. C. Freire, N. Wex, T. M. Tauris, R. S. Lynch, M. H. van Kerkwijk, M. Kramer, C. Bassa, V. S. Dhillon, T. Driebe *et al.*, Science **340**, 1233232 (2013).

[40] B. P. Abbott, R. Abbott, T. D. Abbott, F. Acernese, K. Ackley, C. Adams, T. Adams, P. Addesso, R. X. Adhikari, V. B. Adya *et al.*, Phys. Rev. X **9**, 011001 (2019).

[41] J. Aasi, B. P. Abbott, R. Abbott, T. Abbott, M. R. Abernathy, K. Ackley, C. Adams, T. Adams, P. Addesso, R. X. Adhikari *et al.* (LIGO Scientific Collaboration), Classical Quantum Gravity **32**, 074001 (2015).

[42] F. Acernese, M. Agathos, K. Agatsuma, D. Aisa, N. Allemandou, A. Allocca, J. Amarni, P. Astone, G. Balestri, G. Ballardin *et al.* (Virgo Collaboration), Classical Quantum Gravity **32**, 024001 (2015).

[43] M. C. Miller, F. K. Lamb, A. J. Dittmann, S. Bogdanov, Z. Arzoumanian, K. C. Gendreau, S. Guillot, A. K. Harding, W. C. G. Ho, J. M. Lattimer *et al.*, Astrophys. J. Lett. **887**, L24 (2019).

[44] T. E. Riley, A. L. Watts, S. Bogdanov, P. S. Ray, R. M. Ludlam, S. Guillot, Z. Arzoumanian, C. L. Baker, A. V. Bilous, D. Chakrabarty *et al.*, Astrophys. J. Lett. **887**, L21 (2019).

[45] R. Essick, I. Tews, P. Landry, S. Reddy, and D. E. Holz, Phys. Rev. C **102**, 055803 (2020).

[46] J. E. Lynn, I. Tews, J. Carlson, S. Gandolfi, A. Gezerlis, K. E. Schmidt, and A. Schwenk, Phys. Rev. Lett. **116**, 062501 (2016).

[47] C. Drischler, K. Hebeler, and A. Schwenk, Phys. Rev. Lett. **122**, 042501 (2019).

[48] K. Hebeler and A. Schwenk, Phys. Rev. C **82**, 014314 (2010).

[49] S. Gandolfi, J. Carlson, and S. Reddy, Phys. Rev. C **85**, 032801(R) (2012).

[50] C. Mondal, B. K. Agrawal, M. Centelles, G. Colò, X. Roca-Maza, N. Paar, X. Viñas, S. K. Singh, and S. K. Patra, Phys. Rev. C **93**, 064303 (2016).

[51] B. A. Brown, Phys. Rev. Lett. **85**, 5296 (2000).

[52] See Supplemental Material at http://link.aps.org/supplemental/10.1103/PhysRevLett.127.192701 for details on extracting nuclear parameters from the nonparametric EOSs, including the impact of muons and higher-order terms, and for details on the correlation between L and $R_{\mathrm{skin}}^{^{208}\mathrm{Pb}}$.

[53] G. Baym, C. Pethick, and P. Sutherland, Astrophys. J. **170**, 299 (1971).

[54] R. Essick, P. Landry, A. Schwenk, and I. Tews, arXiv:2107.05528.

[55] C. Drischler, V. Soma, and A. Schwenk, Phys. Rev. C **89**, 025806 (2014).

[56] R. Somasundaram, C. Drischler, I. Tews, and J. Margueron, Phys. Rev. C **103**, 045803 (2021).

[57] N. Chamel and P. Haensel, Living Rev. Relativity **11**, 10 (2008).

[58] J. Tanaka, Z. Yang, S. Typel, S. Adachi, S. Bai, P. van Beek, D. Beaumel, Y. Fujikawa, J. Han, S. Heil *et al.*, Science **371**, 260 (2021).